AIAA 80-0064R

Viscous Flow over Arbitrary Geometries at High Angle of Attack

William S. Helliwell,* Richard P. Dickinson,† and Stephen C. Lubard‡
Areté Associates, Santa Monica, Calif.

A numerical method capable of predicting the supersonic, laminar viscous flow about arbitrary geometries without axial separations at high angle of attack is presented. The approach used is to solve the steady three-dimensional "parabolized Navier-Stokes equations" written in a body-oriented shock-oriented coordinate system. For the complex three-dimensional re-entry vehicle geometries of interest, a nonorthogonal curvilinear coordinate system is developed. The three velocity components are also defined in the nonorthogonal coordinate directions. Predictions using the new approach have been obtained for a blunt biconic with windward and leeward cuts at a Mach number of 10 and angles of attack up to 10 deg. These predictions are compared with experimental data and show good agreement.

Nomenclature

g = $\det(g_{ij}) = g_{11}g_{22}g_{33} - g_{22}g_{13}^2$
g^i = vector orthogonal to g_j and g_k $i \neq j$, $i \neq k$, $(g^i \cdot g_j = \delta^i_j)$
g^{ij} = $g^i \cdot g^j$ $i,j = 1,2,3$
g_{ij} = $g_i \cdot g_j$ $i,j = 1,2,3$
g_1, g_2, g_3 = vectors in ξ_1 streamwise, ξ_2 normal, and ξ_3 circumferential directions, respectively
h = static enthalpy
H = total enthalpy, $H = h + [(\gamma - 1)M_\infty^2/2]\,|V_\infty|^2$
k/C_p = ratio of conductivity and specific heat
M_x = local Mach number $= \sqrt{g_{11}}\,uM_\infty/\sqrt{h}$
M_∞ = Mach number
p = pressure
u, u_1 = tensor velocity component in the g_1 direction
v, u_2 = tensor velocity component in the g_2 direction
V = $\sum_i u_i g_i = ug_1 + vg_2 + wg_3$
w, u_3 = tensor velocity component in the g_3 direction
z, r, ϕ = cylindrical coordinates
α = angle of attack
γ = ratio of specific heats
∇f = $\sum_i g^i \frac{\partial f}{\partial \xi_i}$
δ^i_j = $1\ i=j\quad 0\ i \neq j$
μ = viscosity, Sutherland Law
ξ_1, ξ_2, ξ_3 = computation coordinates
ρ = density, perfect gas law
$\{j^i k\}$ = Christoffel symbol of the second kind

$$\frac{1}{2}\sum_m g^{im}\left[\frac{\partial g_{mk}}{\partial \xi_j} + \frac{\partial g_{mj}}{\partial \xi_k} - \frac{\partial g_{jk}}{\partial \xi_m}\right]$$

All lengths are nondimensionalized by use of a reference length; velocities, density, enthalpy, viscosity, conductivity and specific heats are all nondimensionalized by use of freestream quantities; and pressure is nondimensionalized by twice the freestream dynamic pressure.

Presented as Paper 80-0064 at the AIAA 18th Aerospace Sciences Meeting, Jan. 14-16, 1980; received Feb. 7, 1980; revision received Aug. 12, 1980.

*Consultant.
†Staff Scientist.
‡Senor Scientist. Member AIAA.

Introduction

THIS paper presents a numerical method for obtaining the supersonic, laminar viscous flow about three-dimensional geometries at high angle of attack. In particular, results are presented for blunt biconic bodies with windward and leeward cuts (see Fig 1). The equations used to model the flow are the steady three-dimensional "parabolized Navier-Stokes equations" (PNS), first derived for circular cones by Lubard and Helliwell.[1,2] These equations have been used to predict the flowfield for a variety of different problems, including flow over sharp and blunt cones at angle of attack up to 40 deg,[3-5] flow over spinning cones at angle of attack,[6] and flow over cones with mass transfer and temperature variation at the surface. In addition to these results that were confined to circular cones, some limited results have been obtained for biconic geometries,[7] noncircular cones[8] and the NASA Space Shuttle.[9]

A nonorthogonal curvilinear coordinate system is presented in this paper that appears ideal for the three-dimensional geometries of interest (e.g., Fig. 1). The governing equations are written in terms of this coordinate system, and the three velocity components are defined in the nonorthogonal coordinate directions. This is different from writing the equations in an orthogonal coordinate system and explicitly performing a coordinate transformation as has been done by previous authors.[10-13]

Predictions using the new approach have been obtained for the body illustrated in Fig. 1 at angles of attack up to 10 deg and Mach number 10. Forces and moments, surface pressure, and heat transfer have been compared with wind tunnel data and show very good agreement.

Coordinate System and Equations

Introduction

The steady Navier-Stokes equations are first written in general vector form, and then a particular coordinate system is chosen. One of the coordinates, ξ_1, is chosen in the general axial direction, another, ξ_2, in a direction away from the body, and the third, ξ_3, around the body (Fig. 2). It is assumed that coordinates with these characteristics and that the types of flows to be studied permit the approximations $\partial/\partial\xi_1 \ll \partial/\partial\xi_2$, $\partial/\partial\xi_3$ in the viscous terms. The resulting system is called the parabolized Navier-Stokes equations (PNS).

Coordinates

Validity of the PNS approximations can be obtained for body-conforming coordinate systems, for example, the body normal system used by Lubard and Helliwell[1,2] or the transformed Cartesian system of Schiff and Steger.[10] In addition, truncation errors in the finite difference approximations of derivatives will be reduced if the coordinates change with the flowfield. This can roughly be achieved throughout the flowfield if the shock surface is also a coordinate surface and the ξ_2 coordinate is normal to both the body and the shock. To generate an orthogonal three-dimensional coordinate system with these properties would be a formidable task. If it is permitted that the ξ_1 and ξ_3 coordinates not necessarily be orthogonal, but are orthogonal to the ξ_2 coordinate, then a coordinate system with the above properties can be generated. This nonorthogonality does not unduly complicate the Navier-Stokes equations, as will be seen in the next section.

In summary, a coordinate system is constructed to have the following properties:

1) One coordinate curve is in the general direction of the flow.

2) The body is a coordinate surface ($\xi_2 = 0$).

3) The ξ_1 and ξ_3 coordinates are necessarily orthogonal only at the body.

4) The ξ_2 coordinate is orthogonal to ξ_1 and ξ_3.

5) The bow shock is a coordinate surface ($\xi_2 = 1$).

In order to generate these nonorthogonal coordinates, we start at the body and calculate out to the shock. The surface of the body is written in cylindrical coordinates as

$$r = r(z,\phi) \tag{1}$$

and g_i is defined to be a vector in the ξ_i direction. The coordinate metrics are defined by $g_{ij} \equiv g_i \cdot g_j$. The ξ_1 and ξ_3 coordinates on the body ($\xi_2 = 0$) are generated by using the method outlined by Blottner and Ellis.[14]

The coordinates in the region from the body surface to the shock surface are obtained by taking the cross product $g_3 \times g_1$. If i', j', k' are unit vectors in cylindrical coordinates, then the ξ_m coordinate vectors are given by

$$g_m = \frac{\partial z}{\partial \xi_m} i' + \frac{\partial r}{\partial \xi_m} j' + r \frac{\partial \phi}{\partial \xi_m} k', \quad m = 1,2,3 \tag{2}$$

Defining n as the cross product between g_3 and g_1, and using Eq. (2), we obtain

$$n = n_1 i' + n_2 j' + n_3 k' \tag{3}$$

where

$$n_1 = r\left(\frac{\partial r}{\partial \xi_3}\frac{\partial \phi}{\partial \xi_1} - \frac{\partial \phi}{\partial \xi_3}\frac{\partial r}{\partial \xi_1}\right)$$

$$n_2 = r\left(\frac{\partial \phi}{\partial \xi_3}\frac{\partial z}{\partial \xi_1} - \frac{\partial z}{\partial \xi_3}\frac{\partial \phi}{\partial \xi_1}\right)$$

$$n_3 = \left(\frac{\partial z}{\partial \xi_3}\frac{\partial r}{\partial \xi_1} - \frac{\partial r}{\partial \xi_3}\frac{\partial z}{\partial \xi_1}\right) \tag{4}$$

Now set $(g_2/\sqrt{g_{22}}) = n/|n|$ and again use Eq. (2) to obtain equations for $\partial z/\partial \xi_2$, $\partial r/\partial \xi_2$, and $\partial \phi/\partial \xi_2$. These equations can now be integrated from the body ($\xi_2 = 0$) to the shock in order to obtain z, r, and ϕ as functions of ξ_1, ξ_2, and ξ_3.

With the coordinates constructed in this manner g_2 is always orthogonal to g_1 and g_3 (i.e., $g_{23} = g_{21} = 0$), but g_1 is not necessarily orthogonal to g_3. By setting g_{22} equal to the square of the shock distance, g_2 will be orthogonal to the shock surface, and the shock will correspond to $\xi_2 = 1$. (Note that doing this makes the coordinate system a function of the solution since the shock distance is unknown). Figure 3 illustrates the resulting coordinates away from the body. Once $z(\xi_1,\xi_2,\xi_3)$, $r(\xi_1,\xi_2,\xi_3)$ and $\phi(\xi_1,\xi_2,\xi_3)$ are known everywhere, the metrics g_{ij} can be obtained by differentiation, i.e.,

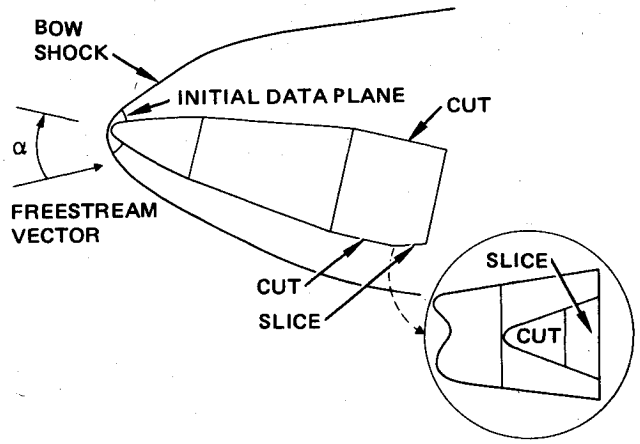

Fig. 1 Typical geometry at angle of attack.

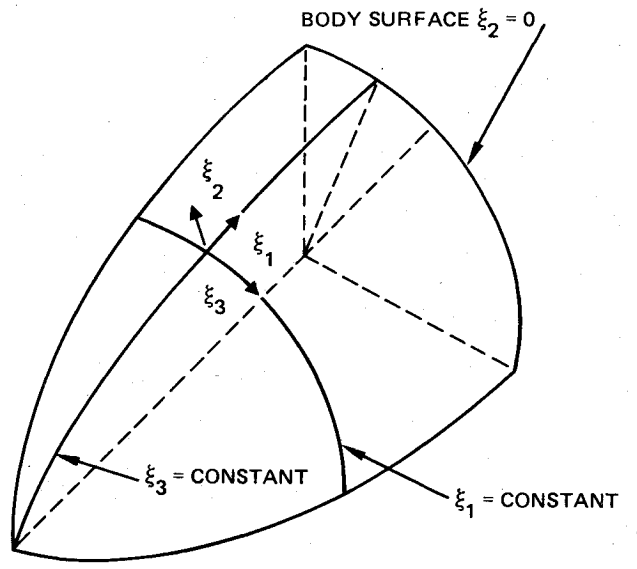

Fig. 2 Coordinate system local to body.

$$g_{ij} = \frac{\partial z}{\partial \xi_i}\frac{\partial z}{\partial \xi_j} + \frac{\partial r}{\partial \xi_i}\frac{\partial r}{\partial \xi_j} + r^2 \frac{\partial \phi}{\partial \xi_i}\frac{\partial \phi}{\partial \xi_j} \quad i,j = 1,2,3 \tag{5}$$

Knowing the metrics, the following important quantities used in the PNS can be computed. These are the determinant of the metric tensor, which for our system is

$$g = g_{11}g_{22}g_{33} - g_{22}g_{13}^2 \tag{6}$$

and the Christoffel symbols of the second kind

$$\{j^i k\} = \frac{1}{2}\sum_{m=1}^{3} g^{im}\left[\frac{\partial g_{mk}}{\partial \xi_j} + \frac{\partial g_{mj}}{\partial \xi_k} - \frac{\partial g_{jk}}{\partial \xi_m}\right] \tag{7}$$

where the g^{ij} are defined by

$$\sum_{k=1}^{3} g^{ik} g_{kj} = \delta_j^i \tag{8}$$

Also, the reciprocal basis defined by

$$g^k = \sum_{i=1}^{3} g^{ki} g_i \quad k = 1,2,3 \tag{9}$$

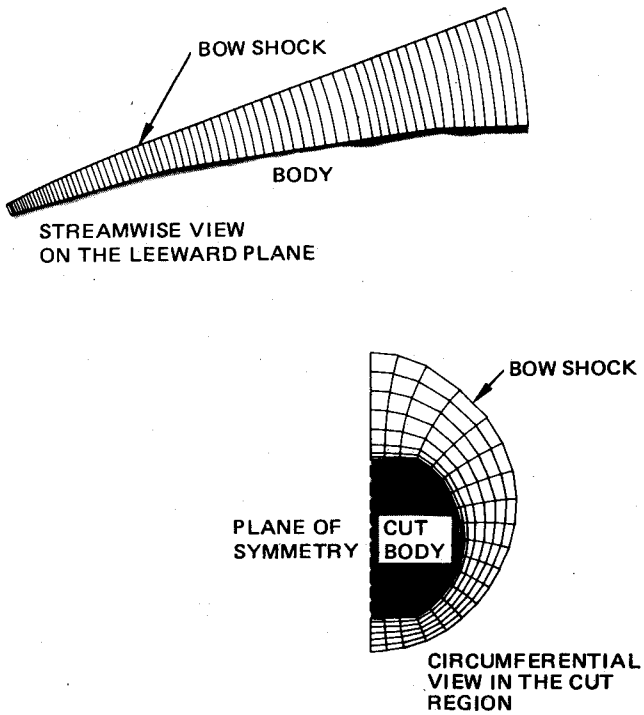

Fig. 3 Body normal-shock normal coordinates.

simplifies the notation.

Parabolized Navier-Stokes Equations

In a general curvilinear coordinate system, the ∇ operator can be written as[15]

$$\nabla = \sum_{k=1}^{3} g^k \frac{\partial}{\partial \xi_k} \tag{10}$$

Starting with the vector form of the Navier-Stokes equations, and conventional tensor analysis the steady Navier-Stokes equations written in nondimensional form, with velocity vector

$$V = ug_1 + vg_2 + wg_3 = u_1 g_1 + u_2 g_2 + u_3 g_3$$

can be written. To simplify notation we define the operator

$$L(f) = \frac{1}{g^{1/2}} \sum_{i=1}^{3} \frac{\partial}{\partial \xi_i} (\rho u_i f g^{1/2}) \tag{11}$$

The equations are

u momentum

$$L(u) + \rho \sum_{i,j=1}^{3} u_i u_j \{i^1 j\} + \frac{g_{22}}{g}\left[g_{33}\frac{\partial p}{\partial \xi_1} - g_{13}\frac{\partial p}{\partial \xi_3}\right] = \mathrm{RHS}_u \tag{12}$$

v momentum

$$L(v) + \rho \sum_{i,j=1}^{3} u_i u_j \{i^2 j\} + \frac{1}{g_{22}}\frac{\partial p}{\partial \xi_2} = \mathrm{RHS}_v \tag{13}$$

w momentum

$$L(w) + \rho \sum_{i,j=1}^{3} u_i u_j \{i^3 j\} + \frac{g_{22}}{g}\left[g_{11}\frac{\partial p}{\partial \xi_3} - g_{13}\frac{\partial p}{\partial \xi_1}\right] = \mathrm{RHS}_w \tag{14}$$

Continuity

$$L(1) = 0 \tag{15}$$

Energy

$$L(h) - (\gamma - 1)M_\infty^2\left[u\frac{\partial p}{\partial \xi_1} + v\frac{\partial p}{\partial \xi_2} + w\frac{\partial p}{\partial \xi_3}\right] = \mathrm{RHS}_e \tag{16}$$

where the right-hand side (RHS) quantities contain all the viscous effects. In these equations, $u(u_1)$, $v(u_2)$, and $w(u_3)$ are tensor velocity components. The physical components are obtained by multiplying by the respective $\sqrt{g_{ii}}$. On the right-hand side of the equations, assuming that $\partial\xi_2$ and $\partial\xi_3$ are $0(Re^{-1/2})$ and that $\partial\xi_1$ along with any derivatives of the metrics are 0(1), and keeping only terms that are 0(1), and using the relation $\lambda = -\frac{2}{3}\mu$, we obtain

$$\mathrm{RHS}_u = \frac{1}{Re}\left[\frac{1}{g_{22}}\left(\frac{\partial \mu}{\partial \xi_2}\frac{\partial u}{\partial \xi_2} + \mu\frac{\partial^2 u}{\partial \xi_2^2}\right) - \frac{g_{22}g_{13}}{g}\left(\frac{\partial \mu}{\partial \xi_2}\frac{\partial v}{\partial \xi_3} + \frac{1}{3}\mu\frac{\partial^2 v}{\partial \xi_2 \partial \xi_3} - \frac{2}{3}\frac{\partial \mu}{\partial \xi_3}\frac{\partial v}{\partial \xi_2}\right) - \frac{1}{3}\frac{g_{22}g_{13}}{g}\left(\frac{\partial \mu}{\partial \xi_3}\frac{\partial w}{\partial \xi_3} + \mu\frac{\partial^2 w}{\partial \xi_3^2}\right)\right.$$
$$\left. + \frac{g_{11}g_{22}}{g}\left(\frac{\partial \mu}{\partial \xi_3}\frac{\partial u}{\partial \xi_3} + \mu\frac{\partial^2 u}{\partial \xi_3^2}\right)\right] \tag{17}$$

$$\mathrm{RHS}_v = \frac{1}{Re}\left[\frac{4}{3g_{22}}\left(\frac{\partial \mu}{\partial \xi_2}\frac{\partial v}{\partial \xi_2} + \mu\frac{\partial^2 v}{\partial \xi_2^2}\right) + \frac{g_{11}g_{22}}{g}\left(\frac{\partial \mu}{\partial \xi_3}\frac{\partial v}{\partial \xi_3} + \mu\frac{\partial^2 v}{\partial \xi_3^2}\right) + \frac{1}{g_{22}}\left(\frac{\partial \mu}{\partial \xi_3}\frac{\partial w}{\partial \xi_2} - \frac{2}{3}\frac{\partial \mu}{\partial \xi_2}\frac{\partial w}{\partial \xi_3} + \frac{1}{3}\mu\frac{\partial^2 w}{\partial \xi_2 \partial \xi_3}\right)\right] \tag{18}$$

$$\mathrm{RHS}_w = \frac{1}{Re}\left[\frac{1}{g_{22}}\left(\frac{\partial \mu}{\partial \xi_2}\frac{\partial w}{\partial \xi_2} + \mu\frac{\partial^2 w}{\partial \xi_2^2}\right) + \frac{4}{3}\frac{g_{11}g_{22}}{g}\left(\frac{\partial \mu}{\partial \xi_3}\frac{\partial w}{\partial \xi_3} + \mu\frac{\partial^2 w}{\partial \xi_3^2}\right) + \frac{g_{11}g_{22}}{g}\left(\frac{\partial \mu}{\partial \xi_2}\frac{\partial v}{\partial \xi_3} - \frac{2}{3}\frac{\partial \mu}{\partial \xi_3}\frac{\partial v}{\partial \xi_2} + \frac{1}{3}\frac{\partial^2 v}{\partial \xi_2 \partial \xi_3}\right)\right] \tag{19}$$

$$\mathrm{RHS}_e = \frac{1}{Re\,Pr}\left[\frac{1}{g_{22}}\left(\frac{\partial}{\partial \xi_2}\left(\frac{k}{C_p}\right)\frac{\partial h}{\partial \xi_2} + \frac{k}{C_p}\frac{\partial^2 h}{\partial \xi_2^2}\right) + \frac{g_{11}g_{22}}{g}\left(\frac{\partial}{\partial \xi_3}\left(\frac{k}{C_p}\right)\frac{\partial h}{\partial \xi_3} + \frac{k}{C_p}\frac{\partial^2 h}{\partial \xi_3^2}\right)\right] + \mu\frac{(\gamma-1)M_\infty^2}{Re}\left\{\frac{g_{11}}{g_{22}}\left(\frac{\partial u}{\partial \xi_2}\right)^2\right.$$
$$+ \frac{g_{11}^2 g_{22}}{g}\left(\frac{\partial u}{\partial \xi_3}\right)^2 + 2\frac{g_{13}}{g_{22}}\frac{\partial u}{\partial \xi_2}\frac{\partial w}{\partial \xi_3} + 2\frac{g_{12}g_{22}g_{13}}{g}\frac{\partial u}{\partial \xi_3}\frac{\partial w}{\partial \xi_3} + \frac{4}{3}\left(\frac{\partial v}{\partial \xi_2}\right)^2 - \frac{4}{3}\frac{\partial v}{\partial \xi_2}\frac{\partial w}{\partial \xi_3} + 2\frac{\partial v}{\partial \xi_3}\frac{\partial w}{\partial \xi_2} + \frac{g_{11}g_{22}^2}{g}\left(\frac{\partial v}{\partial \xi_3}\right)^2$$
$$\left. + \frac{g_{33}}{g_{22}}\left(\frac{\partial w}{\partial \xi_2}\right)^2 + \left(\frac{1}{3} + \frac{g_{11}g_{22}g_{33}}{g}\right)\left(\frac{\partial w}{\partial \xi_3}\right)^2\right\} \tag{20}$$

Boundary Conditions

At the body, the no-slip conditions are used and the enthalpy is specified. Hence,

$$u=0, \quad v=0, \quad w=0, \quad h=\text{specified} \tag{21}$$

To get the surface pressure, the v-momentum equation evaluated at the body is used. This equation becomes

$$\frac{\partial p}{\partial \xi_2}=\frac{1}{Re}\left[\frac{4}{3}\mu\frac{\partial^2 v}{\partial \xi_2^2}+\frac{\partial \mu}{\partial \xi_3}\frac{\partial w}{\partial \xi_2}+\frac{1}{3}\mu\frac{\partial^2 w}{\partial \xi_2 \partial \xi_3}\right] \tag{22}$$

At the plane of symmetry, the ξ_3 velocity component w and the g_{13} metric are antisymmetric, and all other flow variables and metrics are symmetric.

At the shock, the Rankine-Hugoniot jump conditions are used, i.e., conservation of mass, momentum, and energy across the bow shock. In addition, since the shock distance is also unknown, the continuity equation is used as a sixth equation. Using a subscript k for values just inside the shock, the equations are

Conservation of mass

$$v_\infty=\rho_k v_k \tag{23}$$

Conservation of normal momentum

$$p_\infty-p_k+g_{22}v_\infty^2\left(1-\frac{1}{\rho_k}\right)=0 \tag{24}$$

Conservation of tangential velocities

$$u_\infty=u_k \tag{25}$$

$$w_\infty=w_k \tag{26}$$

Conservation of energy

$$h_\infty-h_k+\frac{(\gamma-1)M_\infty^2}{2}g_{22}v_\infty^2\left(1-\frac{1}{\rho_k^2}\right)=0 \tag{27}$$

Continuity

$$\frac{\partial}{\partial \xi_1}(\rho_k u_\infty g_k^{1/2})+\frac{\partial}{\partial \xi_2}(\rho_k v_k g_k^{1/2})+\frac{\partial}{\partial \xi_3}(\rho_k w_\infty g_k^{1/2}) \tag{28}$$

Numerical Solution

The equations are solved by marching in the ξ_1 direction with completely implicit differencing in the ξ_2 and ξ_3 coordinates. The resulting algebraic equations are solved at each ξ_1 step by the Newton-Raphson/Gauss-Seidel iteration method developed by Lubard and Helliwell.[1,2]

A plane of initial condition data downstream of the sonic plane is required in order to obtain the solution using the PNS. At present, the initial conditions are provided by Arnold Engineering Development Center (AEDC) at the sphere-cone tangency point. To get these initial conditions AEDC rotates the solution for axisymmetric flow over a sphere.[11]

The geometries considered have slope discontinuities, none of which were treated in any special way. The body is described in cylindrical coordinates [Eq. (1)] and local body slopes are computed using a backward (two-point) difference in ξ_1 and a centered (three-point) difference in ξ_3. No attempt was made to have coordinate points occur at slope discontinuities, corners were therefore straddled in a random fashion. To determine what effect coordinate location would have on the solution, several computer runs were made over the 14/7 biconic juncture at 10 deg angle of attack. It was found that the solution depends weakly on stepsize (and then only in the immediate vicinity of the juncture) and not at all on the relative location of the juncture to the gridpoints.

An inherent problem with the PNS is the possibility of departure solutions. This characteristic of the equations has been discussed by many authors.[1,2,8,10,12] Suppression of departure solutions depends upon proper numerical treatment of the $\partial p/\partial \xi_1$ term appearing in the equations. In fact, only in the u-momentum equation in the region where the local Mach number is near or less than one does $\partial p/\partial \xi_1$ require special treatment. Many different methods were tried in order to obtain solutions for the geometries considered in this paper.

In particular, one method that was tried was to set $\partial p/\partial \xi_1$ to zero. Solutions could be obtained for all cases in Table 1 over the biconic junctures, however the solution procedure failed immediately upon entering the cut region in case 4. This failure was felt to be due to the fact that $\partial p/\partial \xi_1=0$ is a very poor approximation to the pressure gradient over a large expansion, (and thus the physics were not modeled well), rather than due to departure or convergence problems.

Also, the viscous sublayer approximation $\partial p/\partial \xi_2=0$ referred to by Schiff and Steger[10] was tried. For this approximation it was found that departure solutions developed even on the 7 deg conical portion of case 4. It was possible to delay departure by increasing the size of the region where $\partial p/\partial \xi_2$ was set to zero, but no matter how large the region was the solution would eventually depart.

The method finally adopted is to difference the pressure gradient term backward in ξ_1. Analysis identical to that of Ref. 2 shows that for convergence

$$\frac{\Delta \xi_1}{\xi_1}<\left|\frac{u}{w}\right|\frac{\Delta \xi_3}{\xi_1} \tag{29}$$

must be satisfied. For a cone this reduces to the restriction given in Ref. 2. To avoid departure the restriction

$$\frac{\Delta \xi_1}{\xi_1}>\frac{\left[\frac{Re\,\rho}{2\mu}(1-M_x^2)\frac{\Delta \xi_2 g_{22}}{u\xi_1}\right]}{\left[1-\cos m_2\Delta\xi_2+\frac{g_{11}g_{22}^2\Delta\xi_2^2}{g\Delta\xi_3^2}(1-\cos m_1\Delta\xi_3)\right]} \tag{30}$$

is obtained which again reduces to the corresponding inequality in Ref. 2 for a cone. Here, $m_2=\pi/\xi_2^*, 2\pi/\xi_2^*,\ldots, \pi/\Delta\xi_2$ where $0\le\xi_2\le\xi_2^*$ and $m_1=1,2,\ldots\pi/\Delta\xi_3$ where $0\le\xi_3\le\pi$.

Table 1 Computed and experimental cases

Run	Mach no.	Re_∞/ft	Biconic	T_0, °R	Cut body	T_w, °R	Angle of attack, deg
1	10.1	1.8×10^6	9.3/5	1900	No	1292	2
2	10	1×10^6	14/7	1900	Yes	560	0
3	10	1×10^6	14/7	1900	Yes	560	2
4	10	1×10^6	14/7	1900	Yes	560	10

Based on the argument presented in the Appendix, this expression can be reduced to

$$\Delta\xi_1/\xi_1 > 0.44K_1\xi_2^* \tag{31}$$

where

$$K_1 = Re\left(\frac{\rho}{2\mu\xi_1}\frac{g_{22}}{\partial\mu/\partial\xi_2}\right)_w$$

and ξ_2^* is the value of ξ_2 where $M_x = 1$.

To solve a problem, $\Delta\xi_1/\xi_1$ must be initially chosen to satisfy Eq. (31), then $\Delta\xi_3$ must be chosen so that Eq. (29) is initially satisfied. $\Delta\xi_1$ must then increase as a function of ξ_1 to obtain the converged, nondeparture solution.

Results and Conclusions

The heat transfer, force and momentum coefficients, and surface pressure results of four computed cases (Table 1) have been compared against wind tunnel data obtained by Arnold Engineering and Development Center (AEDC). Selected results for the 14/7 biconic with cuts and slice at 10 deg angle of attack (case 4) are presented here. Figure 4 describes the body geometry used. The body has a plane of symmetry and a nose radius of ½ in. Figure 5 compares the measured and calculated force and moment coefficients for a similar body but with only a windward cut. Excellent agreement between the predictions and the measurements are obtained.

The remainder of the comparisons will be surface pressure and heat transfer results and will be for the exact geometry of Fig. 4.

Figure 6 compares the heat transfer over the biconic and cut regions. The axial distance is measured in inches from the tip of the body. On the windward side and at 90 deg the agreement is very good. On the leeward side up to just past the biconic junction the agreement is also very good, but then the solution starts to diverge from the data. We believe this is due to transition from laminar to turbulent flow. For the $\alpha = 10$ deg case, separation in the circumferential direction first occurs on the 14 deg forecone near the leeside, but presents no running problems for the code.

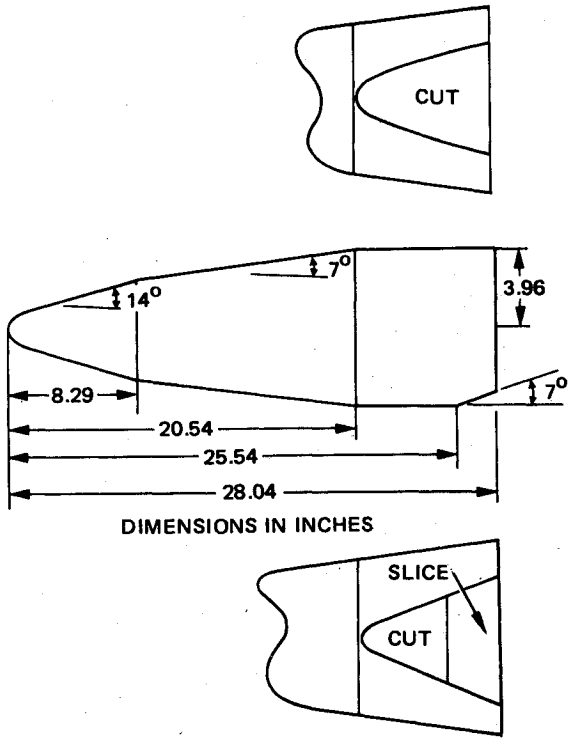

Fig. 4 14/7 biconic with cuts.

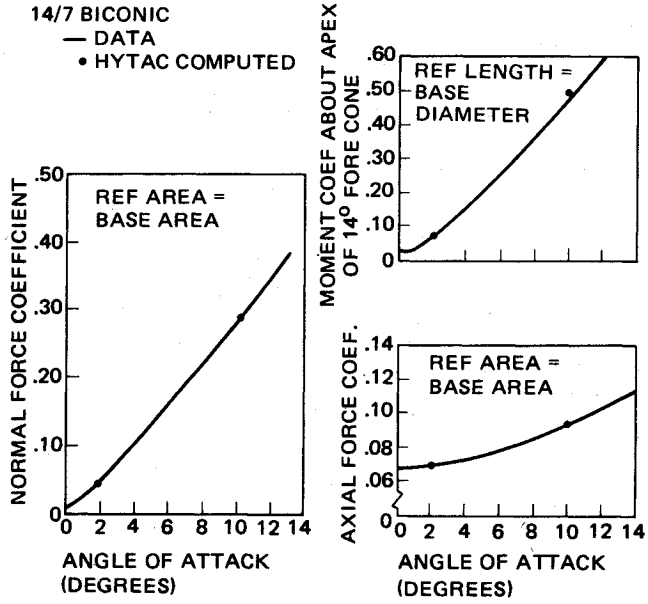

Fig. 5 Force and moment coefficient comparisons for a 14/7 biconic with windward cut only.

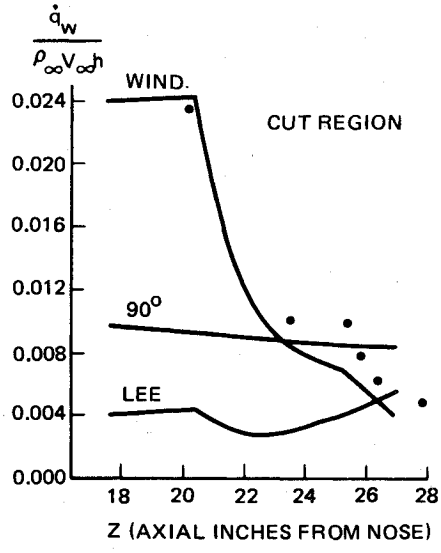

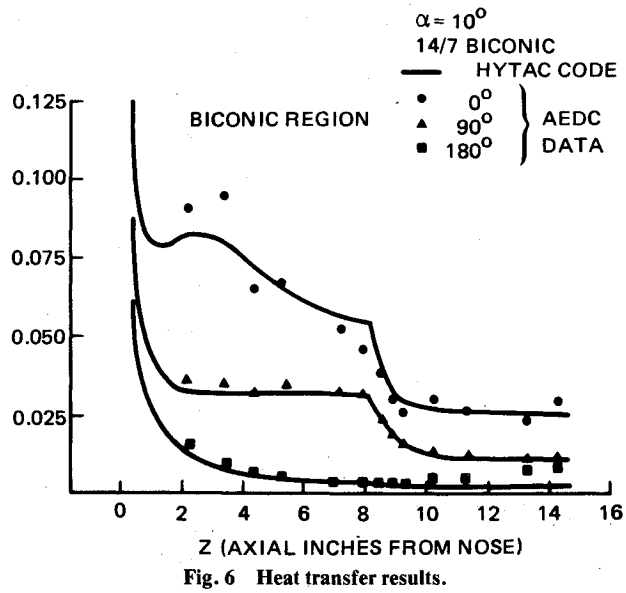

Fig. 6 Heat transfer results.

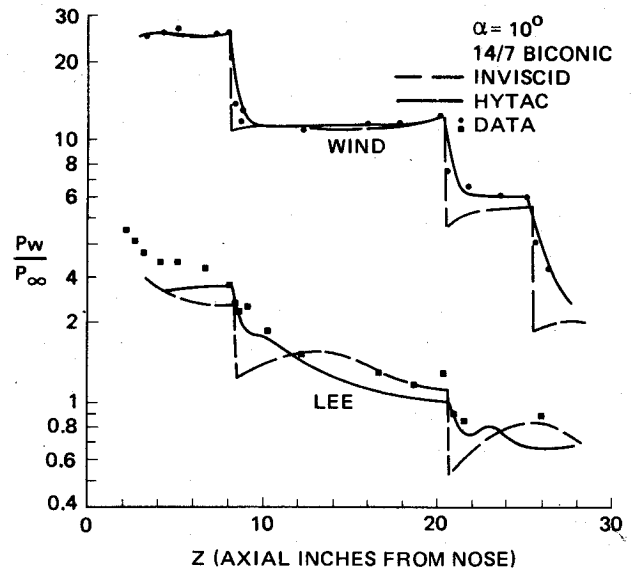

Fig. 7 Surface pressure axial direction.

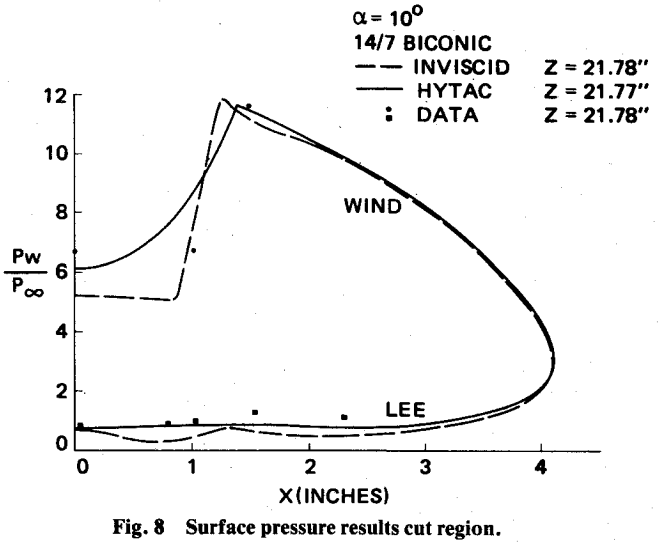

Fig. 8 Surface pressure results cut region.

Figure 7 is a comparison of the wall pressure from the HYTAC calculations and the AEDC data and also an inviscid calculation.[13] The windward side pressures agree quite well, and on the leeward side the data and HYTAC results are also in agreement. The axial distance in this plot is in inches from the tip of the blunt body. Figure 8 is a circumferential plot of the wall pressure and heat transfer comparing the HYTAC results with the data in the cut region at an axial distance of $Z=21.77$ in. (from the blunt nose). In this plot the X axis is in inches from the plane of symmetry of the body. The disagreement between the HYTAC results and the data on the windward side could be due to circumferential resolution. Only two ξ_3 points are on the cut portion of the body at this axial station.

Appendix

To simplify Eq. (30) somewhat, it is sufficient to consider

$$\frac{\Delta\xi_1}{\xi_1} > \left[\frac{Re\rho}{2\mu}\frac{\Delta\xi_2 g_{22}}{u\xi_1}\Delta\xi_2\right] \Big/ \left[1-\cos\frac{\pi\Delta\xi_2}{\xi_2^*}\right] \tag{A1}$$

This restriction is strongest for small u, that is evaluated at $\xi_2=\Delta\xi_2$. With the inequality Eq. (A1) evaluated at $\Delta\xi_2$, $Re\rho/2\mu$ is approximately constant as a function of ξ_1 and $\Delta\xi_2$, and so is $\Delta\xi g_{22}/u\xi_1$. We then have for a constant K_1

$$\frac{\Delta\xi_1}{\xi_1} > \left[\frac{K_1\Delta\xi_2}{1-\cos\left(\frac{\pi\Delta\xi_2}{\xi_2^*}\right)}\right] \tag{A2}$$

where $0<\Delta\xi_2\leq\xi_2^*$. For small $\Delta\xi_2$ this inequality behaves like $1/\Delta\xi_2$. However, keep in mind that the analysis is for constant coefficients and we have permitted u to vary linearly with $\Delta\xi_2$.

Another way to try to determine how the nonlinearity affects Eq. (A1) is to consider that u is less than or equal to u evaluated at $\Delta\xi_2$ only for $\xi_2\leq\Delta\xi_2$. So perhaps in analyzing Eq. (A1) for small u we should take $\xi_2^*=\Delta\xi_2$. In this case Eq. (A1) becomes

$$\Delta\xi_1/\xi_1 > K_1(\Delta\xi_2/2) \tag{A3}$$

Thus, on the one hand, $\Delta\xi_1/\xi_1$ behaves like $1/\Delta\xi_2$ and on the other, like $\Delta\xi_2$. In practice, the behavior is in between these two extremes, that is, $\Delta\xi_1/\xi_1$ is constant as a function of $\Delta\xi_2$. This constant is found by finding the minimum of the right-hand side of Eq. (A2), as a function of $\Delta\xi_2$, for ξ_2^* equal to the value of ξ_2 where $M_x=1$. That is,

$$\Delta\xi_1/\xi_1 > 0.44K_1\xi_2^* \tag{A4}$$

It is seen that to avoid departure $\Delta\xi_1$ must increase with ξ_1. The value of $\Delta\xi_1$ is independent of the grid spacing in the ξ_2 and ξ_3 directions, and is a function of the flow. Also, the right-hand side of Eq. (29) is approximately constant as a function of ξ_1 and so to obtain convergence $\Delta\xi_1$ must increase linearly with ξ_1.

Admittedly, the analysis to obtain inequalities Eqs. (29) and (31) is far from rigorous. Yet, these expressions have been used just as they appear to obtain solutions successfully for a variety of geometries under an assortment of freestream and wall conditions.

Acknowledgments

We would like to acknowledge the support of Drs. Arloe Mayne and John Adams of ARO, Inc., who supplied the initial conditions and inviscid calculations for the sample cases, and Dr. Michael Varner, also of ARO, Inc., who supplied the wind tunnel data used in the comparisons.

References

[1] Lubard, S. C. and Helliwell, W. S., "Calculation of the Flow on a Cone at High Angle of Attack," *AIAA Journal*, Vol. 12, July 1974, pp. 965-974.

[2] Helliwell, W. S. and Lubard, S. C., "An Implicit Method for Three-Dimensional Viscous Flow with Application to Cones at Angle of Attack," *Journal of Computers and Fluids*, Vol. 3, 1975, pp. 83-101.

[3] Adams, J. C., "Numerical Calculation of the Three-Dimensional Hypersonic Viscous Shock Layer on a Sharp Cone at Incidence," *Proceedings 1976 Heat Transfer and Fluid Mechanics Institute*, pp. 340-355.

[4] Lubard, S. C., and Rakich, J. V., "Calculations of the Flow on a Blunted Cone at High Angle of Attack," AIAA Paper 75-149, Pasadena, Calif., Jan. 1975.

[5] Washiewiez, J. D and Lewis, C. H., "Hypersonic Viscous Flows over Sphere Cones at High Angle of Attack," AIAA Paper 78-64, Huntsville, Ala., Jan. 1978.

[6] Agarwal, R. and Rakich, J. V., "Computation of Hypersonic Viscous Flow Past Spinning Sharp and Blunt Cones at High Angle of Attack," AIAA Paper 78-65, Huntsville, Ala., Jan. 1978.

[7] Mayne, A. W., Jr., "Calculation of the Laminar Viscous Shock Layer on a Blunt Biconic Body at Incidence to Supersonic and Hypersonic Flow," AIAA Paper 77-88, Los Angeles, Calif., 1977.

[8] Vigneron, Y. C., Rakich, J. V., and Tannehill, J. C., "Calculations of Supersonic Flow over Delta Wings with Sharp Leading Edges," AIAA Paper 78-1137, July 1978.

[9] Agopian, K. G., Collins, J., Helliwell, W., Lubard, S. C., and Swan, J., "NASA Viscous 3-D Flowfield Computations," R&D Associates Tech. Rept. RDA-TR-5100-007, Oct. 1975.

[10] Schiff, L. B. and Steger, J. L., "Numerical Simulation of Steady Supersonic Viscous Flow," AIAA Paper 79-0130, New Orleans, La., Jan. 1979.

[11] Mayne, A. W., Jr., "Calculation of the Laminar Viscous Shock Layer on a Blunt Biconic Body at Incidence to Supersonic and Hypersonic Flow," AIAA Paper 77-88, Los Angeles, Calif., 1977.

[12] Rakich, J. R., Vigneron, Y. C., and Agarwall, R., "Computation of Supersonic Viscous Flows Over Ogive-Cylinders at Angle of Attack," AIAA Paper 79-0131, New Orleans, La., 1979.

[13] Marconi, F., Yaeger, L., and Salas, M., "Development of a Computer Code for Calculating the Steady Super-Hypersonic Inviscid Flow Around Real Configurations," Vols. I and II, *Computational Techniques*, NASA, CR-2675 and CR-2676.

[14] Blottner, F. G. and Ellis, M., "Three-Dimensional, Incompressible Boundary Layer on Blunt Bodies," Sandia Laboratories, SLA-73-0366, April 1973.

[15] Sokolnikoff, I. S., *Tensor Analysis Theory and Applications to Geometry and Mechanics of Continua*, John Wiley and Sons, Inc., New York, 1964.